Resistance of alkali-activated grouts to acid leaching

Anass Cherki El Idrissi, Emmanuel Rozière, Sabine Darson-Balleur, Ahmed Loukili

Resistance of alkali-activated grouts to acid leaching

Anass Cherki El Idrissi[a], Emmanuel Rozière[a], Sabine Darson-Balleur[b], Ahmed Loukili[a]

[a] Université Bretagne Loire, Ecole Centrale de Nantes, Institut de recherche en Génie civil et Mécanique (GeM) – UMR CNRS 6183, 1 rue de la Noe, 44321, Nantes cedex 3, France

[b] Soletanche Bachy, Chemin des Processions, 77130, Montereau Fault-Yonne, France

Abstract

At very low pH values materials based on hydraulic binders cannot be directly exposed to acid solutions due to leaching, hence the need for additional coatings. As these are generally characterized by relatively high cost and environmental impact, new solutions are being developed. In this study, grouts based on alkali-activated materials (activated slag and activated metakaolin with and without fly ash) have been considered as an alternative to be directly exposed to acid solutions at pH = 3.5, and compared with slag cement grout. The direct monitoring of mass and volumes was combined with the chemical analysis of the leachate and the observations of cross sections through SEM/EDS and X-ray tomography in order to understand the mechanisms involved in the leaching of studied materials. The cumulated amount of leached ions was converted into an equivalent mortar volume loss and compared with the direct measurement of the volume loss. A good correlation was found for slag cement and activated metakaolin, as leaching mainly affected the binding phase. For activated slag the volume loss was lower than expected due to the formation of new phases such as silica-rich gel. The higher volume loss of metakaolin-fly ash grout was attributed to the influence of partially reacted fly ash particles.

Keywords: Leaching, acid attack, alkali-activated materials, slag, metakaolin

1. Introduction

Leaching consists in the progressive dissolution of a solid material through the action of a percolating liquid. Its consequences depend on multiple chemical and environmental parameters such as pH, temperature, liquid/material ratio and the mobility of the leaching medium (still or flowing) [1, 2]. The loss of leached elements is likely to weaken the binding phase, which affects its mechanical properties [3] and eventually leads to the complete failure of the material [4]. In severe environmental conditions, the resistance to leaching is a decisive parameter in the choice of the material to be used.

In Portland cement-based materials, leaching mainly affects the behavior of calcium-rich hydration products [5]. Portlandite ($Ca(OH)_2$) is usually the first phase to be dissolved in the process [6,7]. This releases calcium cations as well as hydroxides. Since leaching is a diffusion-dissolution phenomenon [8], the dissolution of portlandite causes an increase in porosity which favors the penetration of the environmental water into the material [9]. Once portlandite is exhausted, the decalcification of the calcium silicate hydrates (C-S-H) can occur. As the C-S-H are the main contributor to mechanical strength, their decalcification weakens the material and causes irreversible damage to its microstructure [10]. Other phases are then dissolved as the front of attack goes further.

The process is significantly accelerated in acid waters, since the added H_3O^+ ions actively participate in the attack through a faster destruction of the chemical bounds [11]. Consequently, the pH of the interstitial water can be a limiting factor to the use of traditional cement-based materials, especially in soil reinforcement and underground structures. The EN 206 European Standard allows implementing performance-based tests and specifications for the durability of concrete. The French standard P18-011 is referred to in NF EN 206-1 standard. According to P18-011, cement-based materials cannot be directly exposed to

environments of pH lower than 4 without any coating [12]. However, near contaminated and industrial sites, as well as in specific exposures, the acidity of the underground water can be even more aggressive. Additional coatings need to be installed [13]. This dramatically increases the cost and complexity of such projects.

Extractive industries are likely to cause some situations where huge volumes of soils need to be contained to avoid the pollution of water resources and the loss of biodiversity. For instance, acid mining drainage consists in the drainage of acid water containing dissolved metals as a result of natural oxidization of sulphides found in waste rock, ore and tailings exposed to air and water [14]. Cement grouts can be used to improve the mechanical and physical properties of soils and rocks. They allow reducing their permeability for containment purposes. They are directly exposed to aggressive waters [15]. In this context, grouts based on alkali-activated materials (AAM) have been considered as a possible alternative to traditional solutions. Sometimes highlighted for their environmental advantages, the main interest of alkali-activated materials remains their better durability in multiple aggressive situations [16, 17]. Their acid resistance has been studied by several authors for different applications.

At the macroscopic level, the main indicators of the resistance to acid leaching are weight loss, decrease in compressive strength, and damaged depth. These consequences are not specific of acid attack, thus most of studies include a characterization of the microstructure and nanostructure of corroded and corroded samples [18]. The weight loss and the strength decrease are both due to the degradation of binding phases. The main phases produced by alkali-activation are the sodium aluminosilicate hydrate (N-A-S-H) gel, and the aluminum-modified calcium silicate hydrate (C-A-S-H) gel with different Ca/Si ratios, depending on the calcium content of aluminosilicate precursors [19]; $Ca(OH)_2$ and AFm can also be observed at higher calcium contents. The resistance to acid leaching was found to depend closely on microstructure and nanostructure. Denser matrices are characterized by lower diffusivity,

which delays the detrimental effects of leaching [20]. The effect of acid attack also depends on the chemical structure of the matrix. Calcium-rich phases are vulnerable to leaching due to their possible decalcification [21]. As a consequence, the replacement of Portland cement by mineral additions such as slag and fly ash generally results in better resistance to acid leaching due to a denser microstructure as well as a lower calcium content [22]. N-A-S-H gel can be affected by the exchange reaction of sodium and hydronium ions [23], and the loss of aluminate from the aluminosilicate network ("geopolymer" gel) or the amorphous phase of high-alumina fly ash [24]. Zhang et al. [18] actually observed that the Al/Si ratio was lower in the corroded layer after acid attack, and this reduction increased with fly ash/slag ratio. The alkali-activation of metakaolin and fly ash mainly results in N-A-S-H gel, whereas activated slag mainly consists of C-A-S-H gel [25, 26]. Even if cement-based and alkali-activated materials are both eventually affected by acid leaching, most of studies mention that alkali-activated materials with low-calcium content show better resistance. Sodium ions are easily leached from the nanostructure of N-A-S-H gel, where they balance the Al negative charges, but this does not affect much the strength of the material [18, 27], as the negative charge can be compensated by the H_3O^+ ions provided by the acid solution. Koenig et al. [28] studied several materials over a wide range of calcium contents. They actually observed that N-A-S-H (low-calcium AAM and geopolymer) had better resistance than C-A-S-H (calcium-rich single or multicomponent AAM), and C-S-H (Portland cement). They suggested a CaO limiting value of 10% in mass to distinguish low-calcium and high-calcium alkali-activated binders.

Several studies focused on the evolution of the mechanical and macroscopic properties when exposed to different types of acid attacks, such as nitric acid [23, 29, 30] and sulfuric acid [31 32]. Organic acids, such as acetic acid [31, 33], cause a more severe damage compared to so called ''strong'' acids, such as sulphuric or hydrochloric acid, because of the acid buffer action and the high solubility of the reaction products [34, 35]. Alkali-activated slag

performed better than Portland cement-based material, even in acetic acid [34]. Damage mechanisms are strongly dependent on the applied acid solution. Several experiments actually induce couplings between acid attack and other degradation mechanisms, such as sulfate attack and chloride ingress. Even if there are correlations between the resistance to leaching and chemical stability [22], each mechanism implies different chemical reactions thus different phases are formed with different consequences on microstructural and engineering properties. Organic acids are relevant for biogenic acid attack in sewage or agricultural concrete applications [36]. Sulfuric acid is also often used to represent sewer conditions. Sulfate-rich phases such as gypsum have been observed in alkali-activated materials exposed to sulfuric acid [18, 20, 37]; Gu et al. [38] also mentioned the development of a barrier of expansive products. Vafaei et al. [39] studied several materials including AAM; H_2SO_4 attack caused more deterioration than HCl attack due to the accelerating effect of gypsum formation. The sulfate resistance of AAM was also generally found to be better than Portland cement systems [40], but sulfuric acid does not seem appropriate to study only acid leaching.

A better understanding of the damage mechanism of alkali-activated materials has also been achieved through chemical analyses of the leachate and damaged samples [41]. Keulen et al. [42] used nitric acid and controlled pH to determine element release as a function of leachate pH. The analysis of the leachate actually allows investigating the leaching of metals [42, 43] or naturally occurring radionuclides [44] from alkali-activated slag. The links between the chemical evolutions and macroscopic indicators have not been sufficiently discussed.

The specifications on fresh cement grouts include low viscosity as they are meant to be injected in soils [45]. Low viscosity implies relatively high water-to-binder ratios. In the case of cement-based materials, the rheological performances can be enhanced through chemical admixtures [46, 47]. This allows finding compromises between low viscosity and low permeability. The increase of water-to-cement ratio actually has a detrimental effect on the

permeability and the resistance to leaching [20, 48]. Cement grouts used for the containment of acid waters had higher w/c; Sephton et al. [15] studied grouts with w/c between 0.8 and 1.2. Moreover, the rheological properties of fresh alkali-activated grouts cannot be improved through the same strategy based on chemical admixtures due to the higher alkaline content of the grouts [49-51]. Existing studies mainly focus on alkali-activated materials with relatively low water-to-solid ratios. However, the use of grouts for soil improvement and containment of aggressive waters leads to consider the behavior of alkali-activated materials with relatively high water-to-solid ratios.

This paper presents a comprehensive study of the resistance of alkali-activated grouts to leaching in acid conditions. First the experimental program is presented. The specimens were immersed in regularly renewed solutions of demineralized water at a constant pH of 3.5 controlled by automatically adding nitric acid. The testing procedure was designed to achieve well-defined exposure conditions, in order to better understand the basic phenomena involved in the degradation mechanism. Through the coupling of multiple characterization techniques (SEM/EDS, X-Ray tomography, chemical analyses) with macroscopic monitoring of mass and volume, a multi-parameter comparison of different mixes has been performed. Metakaolin, metakaolin-fly ash and slag mixtures are studied, compared to a reference Portland-Slag cement grout. Then the results are presented, first macroscopic indicators, then the direct observation of cross-section, and chemical analyses. Finally the correlations between macroscopic indicators and chemical parameters are plotted and discussed.

2. Materials and methods

2.1 Materials, mixing, and curing

The physical and chemical properties of the materials are given in Table 1. The analysis of specific surface of slag, metakaolin and fly ash was performed from Brunauer, Emmett et

147 Teller (BET) theory. The packing density of powders was determined from their water
148 demand using the flow spread test. Commercially available products were used to design the
149 studied mixtures. Slag cement CEM III/C with high slag content (85 %) was chosen here as it
150 is often recommended to design grout mixtures for chemically aggressive environments.
151 Binders with high slag content actually show relatively good behavior in pure or acid water
152 [52]. Metakaolin was obtained from flash calcination of clay from Fumel, France. Low-
153 calcium fly ash was produced from thermal power plant in Hornaing, France. Sodium silicate
154 had a SiO_2/Na_2O molar ratio of 1.7, a dry matter content of 44% and a density of 1.57.

155 **Table 1.** Chemical composition and physical properties of materials

	Slag cement	**Slag**	**Metakaolin**	**Fly ash**
(Mass, %)				
Total SiO_2	31.7	37.2	67.1	50.0
Total Al_2O_3	9.5	10.5	26.8	20.0
CaO	44.8	43.2	1.1	1.0
Fe_2O_3	0.8	0.6	2.6	8.5
MgO	6.6	7.0	0.1	3.0
SO_3	3.1	0.1	-	0.6
TiO_2	0.5	0.5	1.3	1.0
Na_2O	0.2	0.6	0.0	0.6
Slag content (%)	85	100	0	0
Density (10^3 kg/m^3)	2.92	2.89	2.63	2.24
Median diameter (µm)	-	10	18	38
BET (m²/g)	-	0.45	16.50	1.24
Packing density (Vol., %)	-	44.4	43.9	62.6

156

157 The compositions of the studied mixtures are given in Table 2. The grouts were designed
158 keeping a constant water-to-solid mass ratio of 0.75. As revealed by specific surface BET
159 (Table 1), the internal porosity of metakaolin was high, thus relatively high water-to-cement
160 ratio was needed to achieve required flowability. The replacement of metakaolin by fly ash
161 improves the rheological properties [53]. The study has been carried on mortars made with

these grouts and 0/2 mm quartz sand from Palvadeau, France. The volume fraction of sand was kept constant at 47%. The grouts were prepared in a high-shear mixer, by dissolving the powders to the activating solution and water in the case of cement. This solution was prepared by diluting a commercial sodium silicate solution in demineralized water, and adding sodium hydroxide in pellet form. The grouts were then mixed with the sand in a mortar mixer. For each mixture, five 20x20x160 mm^3 specimens were prepared and stored under plastic film for 7 days at 20 ±1°C. Then, one centimeter of each extremity was coated with resin to avoid damage near the measurement inserts. The specimens were stored under water until testing.

Table 2. Compositions of the studied grouts and origins of the materials (g/L)

	Type	C3	AS	AM	AMF
Cement	CEM III/C 32.5	923.1	-	-	-
Slag	GGBFS	-	739.8	-	-
Metakaolin	Flash calcination	-	-	670.9	402.5
Fly ash	Type F	-	-	-	228.6
Sodium silicate	Commercial	-	454.2	583.0	583.0
Sodium hydroxide	Pellets, 98.5%	-	3.0	3.0	3.0
Water	Demineralized water	692.3	450.0	366.7	366.7

2.2 Experimental procedures

28 days after mixing, two samples were immersed in demineralized water for acid exposure, under permanent magnetic stirring and controlled temperature of 20°C, and the three other specimens were stored in water as control samples. The pH of each cell was individually controlled at 3.5 using 0.5M nitric acid [52, 54]. The added volume of acid was periodically monitored, at least once daily, and samples of the solutions were extracted after every renewal. The solution was renewed at fixed intervals of added volume of acid (every 40 ml during the first testing week, 20 ml later) in order to maintain the gradient of concentrations between the acid solution and the pore solution. Samples of the demineralized water were also

taken before the immersion of mortar samples to establish a baseline for the chemical analysis. With each renewal, the saturated surface dry mass of the samples was measured, along with their volume variation via hydrostatic weighing. The same measurements were carried on control samples kept in demineralized water in order to assess relative variations of monitored parameters. The leachate solutions as well as the water samples were analyzed in a certified lab for the quantification of six ions: silicon, aluminum, calcium, sodium, magnesium, and iron.

The mass and volume of control and tested specimens, and added acid volume, were monitored for 120 days. Then the central part specimens exposed to acid attack was sawn to extract two prismatic samples for SEM-EDS and X-ray microtomography. The detailed conditions of these observations and analyses are given in [55].

3. Results and discussion

3.1 Macroscopic evolutions

As the studied mortars were exposed to acid attack in four different cells, the control of pH directly provides the first indication of the degradation of the materials through the cumulated amount of added acid. The H_3O^+ cations provided by the nitric acid actually neutralize the OH^- ions leached from the pore solution of samples (equation 1).

$$H_3O^+ + OH^- \rightarrow 2H_2O \qquad \text{Equation (1)}$$

The average quantity of leached OH^- ions can be deduced from the cumulated volume of acid. In Fig. *1*, this quantity is plotted against the square root of time. The curves are quasi-linear, showing that the mechanism of degradation is based on diffusion and dissolution [10, 52]. The slope of each curve is an indicator of the leaching kinetics, which provides a first

classification of the studied samples. AM and AMF samples underwent a slower leaching process (4.6 and 7.0 mmol/√day) than C3 and AS (12.7 and 11.2 mmol/√day).

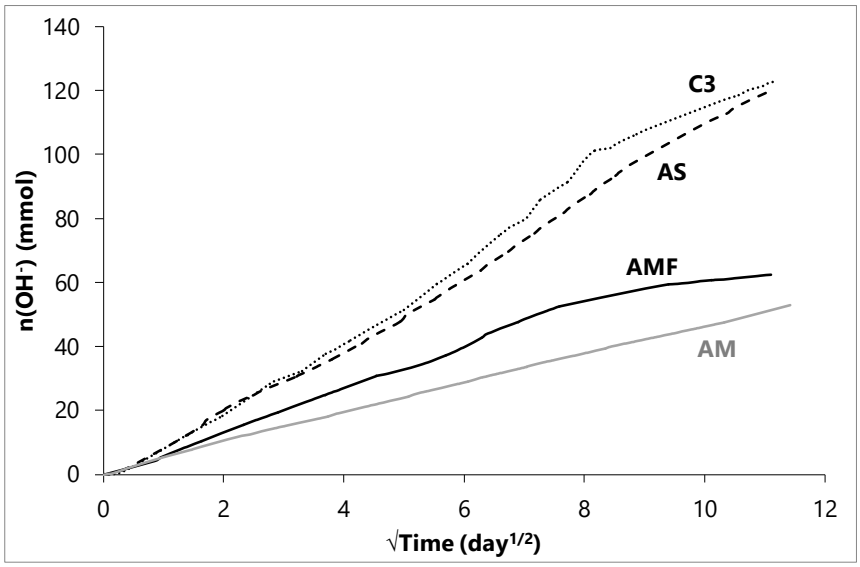

Fig. 1. Leached OH^- ions as a function of the square root of time

The mass and volume losses calculated from measurements after 120 days are presented in Table 3. The ranking is the same as the leaching kinetics. The significant mass loss of the C3 samples (8 % in 4 months) can be associated to the weakened binding phases and the subsequent loss of sand particles. In the AM samples, the mass loss was very low (less than 1 %), confirming the good stability of metakaolin geopolymers in these conditions [56]. The mass loss of AMF samples was higher, which could be explained by the presence of unreacted FA particles that lower the effective binder content and add more inclusions to the material [57]. The average volume loss of the samples after 120 days partly confirms the trends given by the mass losses. The volume decrease of C3 samples was significant. AM showed good volume stability, which is consistent with the quasi absence of degradation observed on the surface of the samples. The results given in Table 3 also indicate a discrepancy between mass and volume variations of AS and AMF specimens. Their volume loss was lower than their mass loss, and their behavior was different from C3 and AMF

specimens. AMF showed approximately the same volume variation as AS, in spite of much lower leaching kinetics. AS showed relatively lower volume variation, or conversely C3 showed high volume variation. The "mass" variations refer to the mass of specimens at SSD state (saturated, dried surface); this volume includes porosity. The "volume" variations refer to the volume of solid phases determined from buoyancy method. The relatively low volume loss of AS implies that new phases had formed in the porosity of the specimens. One can also consider that the mass decrease of C3 specimens was higher than expected from volume variations, which allows assuming that the porosity of the sample increased. The same phenomena could have occurred in AMF and AM respectively. The discrepancies between mass and volume variations could also originate from the density of dissolved or lost phase, which can significantly differ from the average density of the material. Thus it is not possible to conclude from mass and volume data to explain the behavior of studied materials. Further analyses were needed to check these hypotheses.

Table 3. Mass and volume losses after 120 days of leaching

Mixes	**C3**	**AS**	**AM**	**AMF**
Mass loss (%)	8.0	4.4	0.9	3.6
Volume loss (%)	8.6	2.4	0.3	2.2

X-ray microtomography can be used to assess the extent of damage within the samples. Cross sections of the specimens are presented in Fig. *2*.

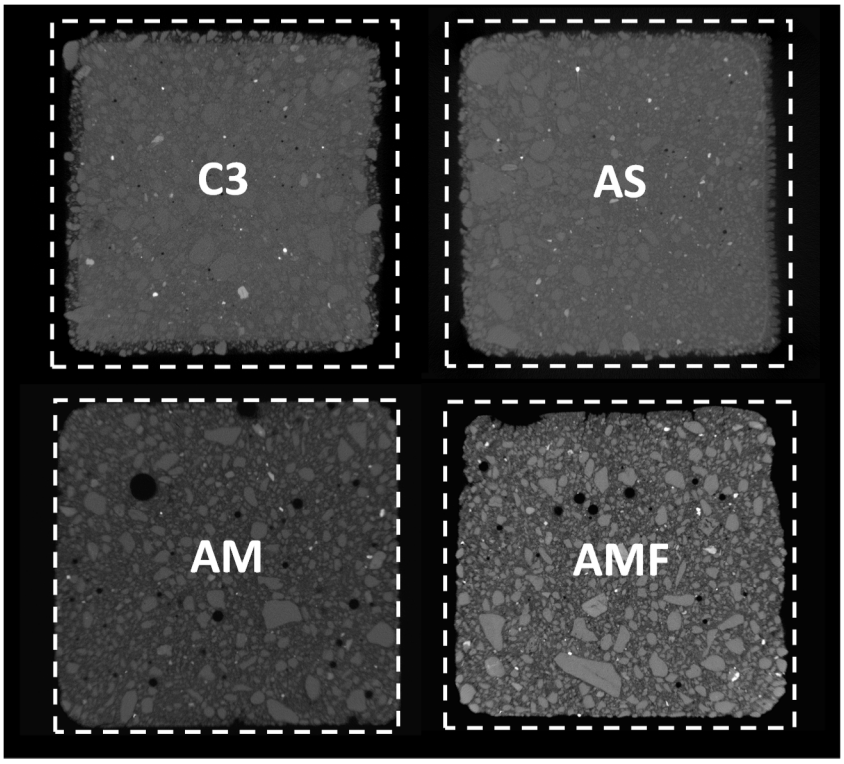

Fig. 2. X-ray micro-tomography scans of the samples and initial section (dashed lines)

As the ends of prismatic specimens were protected by an acid resistant resin, leaching was mainly two-dimensional. The degradations observed on cross-sections can be used to understand the mass and volume variations. In the AM and AMF samples, the binding matrix remained homogeneous with no signs of cracking or increased porosity. The AMF picture shows a seriously altered outer surface attributable to the significant loss of sand and FA particles. The damaged zone in the outer part of C3 sample reveals an increase in porosity. A significant proportion of the matrix has been dissolved, accompanied by the loss of sand particles. The AS sample shows a similar aspect but the reduction of cross section and the depth of damaged zone are lower. The information provided by microtomography is consistent with mass and volume variations provided by direct measurements. AM showed good stability, C3 showed the highest volume and cross-sections losses, and AS and AMF intermediate behaviors.

This is consistent with the works stating a better resistance of activated slag than Portland cement to acid environments [33, 58]. Shi and Stegemann [59] attributed the difference to the nature of reaction products present in each material. The main products in activated slag are calcium silicate hydrates (C-S-H) with a low Ca/Si ratio, while cement paste contains higher Ca/Si C-S-H accompanied by $Ca(OH)_2$. Since decalcification is the main degradation mechanism, hydrated cement is more vulnerable to acid exposition and displays stronger effects. Mellado et al. [30] reported that the alkali-activated materials with the lowest calcium content lead the best performance.

3.2 Chemical analyses and microstructural characterization

The increase in porosity of C3 sample could explain its relatively high volume loss (Table 3). However, this variation needs to be quantified thus chemical data were used to identify the leached or precipitated species. The damaged zone in C3 has been examined via SEM/EDS (Fig. *3*).

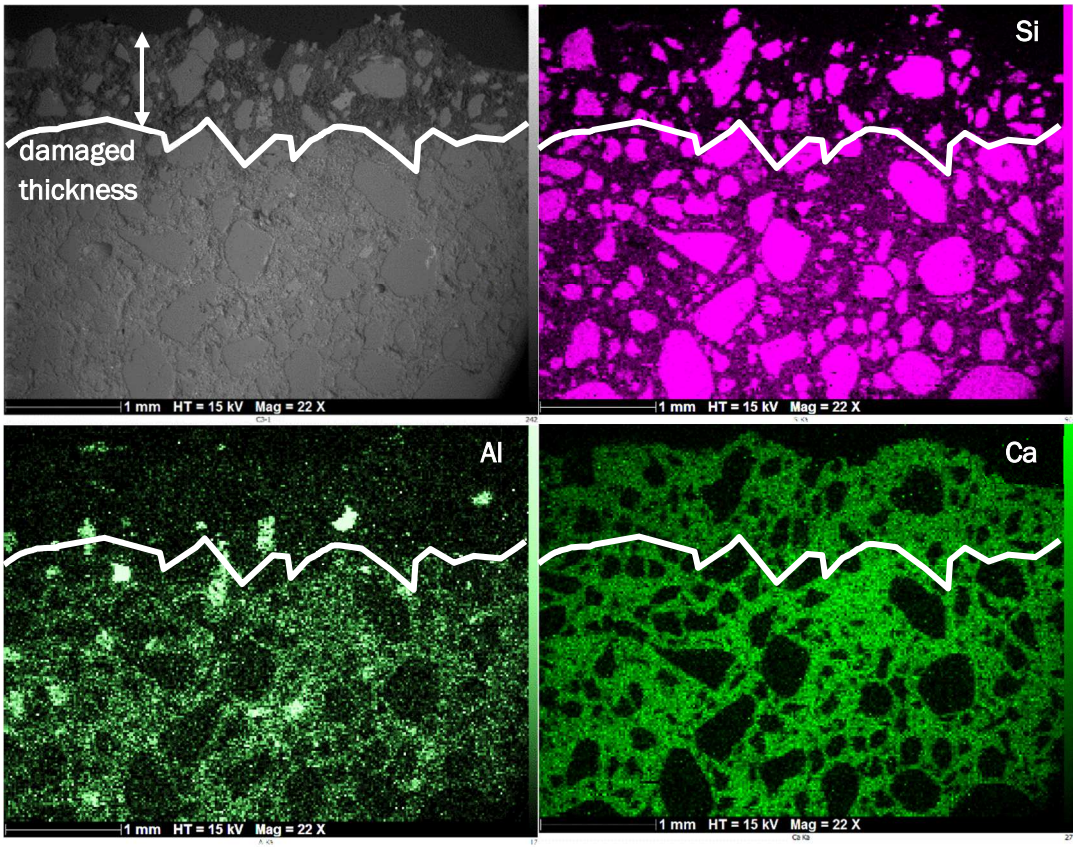

Fig. 3. SEM/EDS scan of the C3 sample showing the damaged zone

Keeping in mind that the outer edge has been eroded to some degree, the remaining interfacial zone shows a distinct discoloration. Confirming the microtomography observations, signs of increased porosity and loss of binder are visible. This weaker part of the sample also shows a lower concentration of structural elements such as silicon, aluminum and calcium. In cement-based materials, these elements are actually the main constituents of hydration products such as C(A)SH, $Ca(OH)_2$, AFm, and calcium aluminate hydrates. These products have different solubility thus different dissolution fronts should theoretically be observed [60]. Here a common front can be distinguished between the damaged and the sound parts of the C3 sample, indicating the extent reached by the acid attack after 4 months. In the damaged zone, the loss of binding phases is likely to accelerate the degradation of the material in the case of coupled phenomena such as carbonation, chloride or sulfate ingress [22]. Weakened binding phases and an increase in porosity seem to be the main factors behind this alteration, as stated

by Beddoe and Dorner [11]. In our study, the higher water/cement ratio (0.75) leads to a relatively high porosity and weaker hydrates, causing favorable conditions for the diffusion and ions exchange between the pore solution and acid environment.

The SEM/EDS analysis of AM also reveals the leaching of each element with some differences in the extent (Fig. *4*). While Si seems barely affected by the acid attack, other elements such as Al and especially Na show a significant variation in their concentration between the edge and the core of the sample. Sodium appears to be the most mobile species, as it is mostly present in the pore solution [61] and it is not covalently bonded to the aluminosilicate network [62]. Aluminum is less present in the outermost part of the sample.

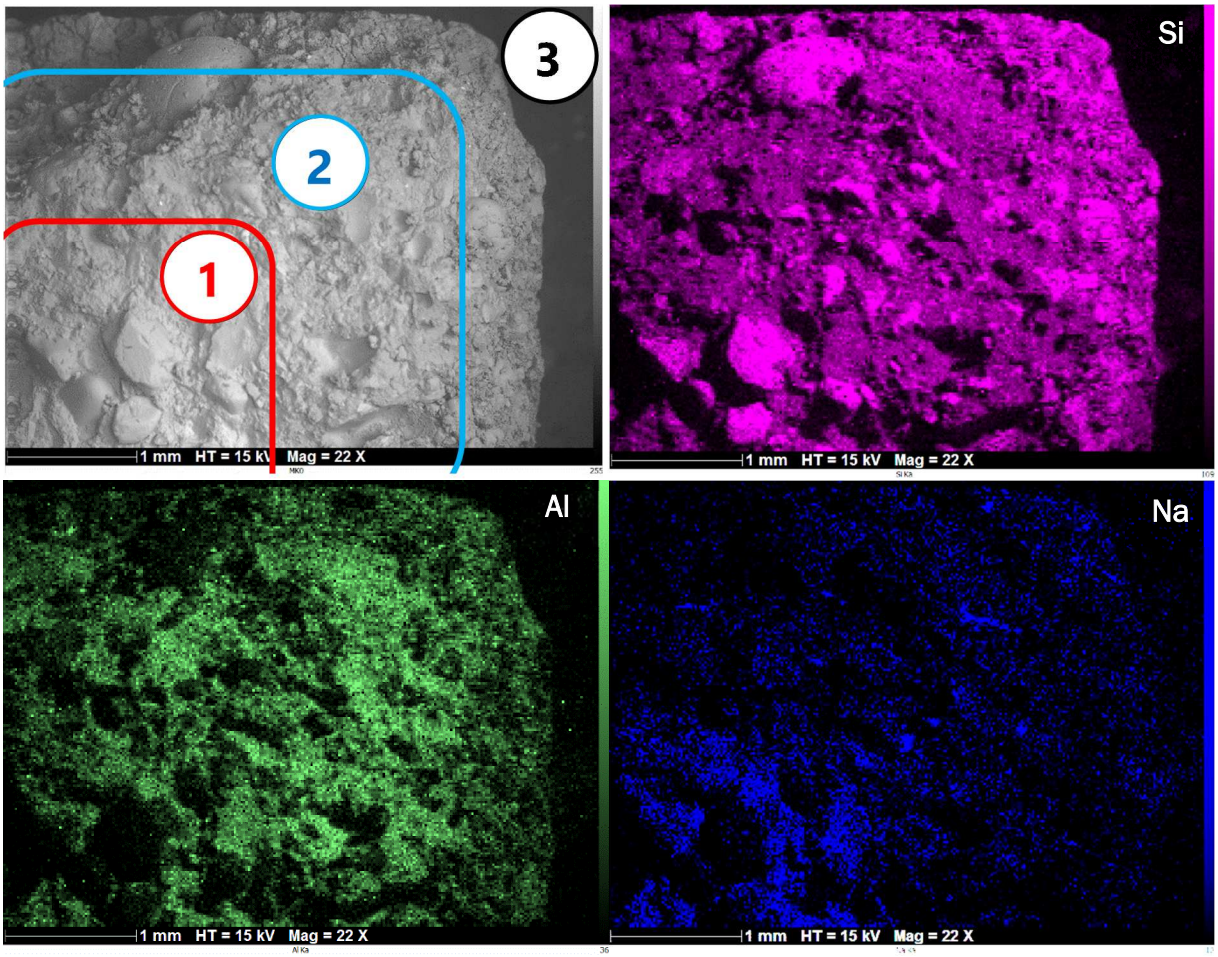

Fig. 4. SEM/EDS scans of the AM sample

The three elements have different leaching kinetics and they have been shown to follow the same pattern in different pH and temperature conditions by Aly et al. [63]. The sample can thus be separated into three distinct areas as shown on the picture in Fig. *4*. In the zone (3), lower aluminum and sodium contents are observed, showing a partial modification of the chemical components of the aluminosilicate network. Zone (2) displays initial concentration of aluminum, whereas sodium content has significantly decreased. The limit between zones (1) and (2) can be considered as the diffusion front of acid into the material. While not presented in this paper, the AMF sample analysis did not show a similar pattern. This is likely due to the erosion that affected the damaged thickness as soon as the network lost its aluminum ions.

The results presented above show different leaching kinetics of the chemical elements. To study this aspect, a sample of the leachate was extracted at every renewal of the solution and analyzed for six elements: Aluminum, Silicon, Calcium, Sodium, Magnesium and Iron. As the initial content depends on the studied mixture, a representative quantity has been used to compare the leaching kinetics of different materials for a given element. The equivalent damaged thickness (EDT) represents the ratio of leached material to the initial quantity, normalized by the area exposed to the attack. It is individually calculated for each of the six elements following equation (2)

$$EDT(m) = \frac{\frac{n_{leached}(mol)}{A_{exp}(m^2)}}{C_{ini}(mol/m^3)} \qquad \text{Equation (2)}$$

where $n_{leached}$ is the leached ion content, A_{exp} is the exposed area of the sample and C_{ini} is the initial content in the mixture. The values of the EDT after 120 days are summarized in Table 4. By comparing the different values, it is noticeable that almost all the leached ions followed the same tendency, with some variations in the ranking of the mixtures. Again, C3 presents the highest leaching rates. The samples mainly lose calcium, which is tightly linked to the

313 dissolution of portlandite and the decalcification of C-S-H in cement-based materials [11, 52],
314 but also considerable amounts of silicon and aluminum. This indicates damaged calcium
315 aluminosilicate (C-A-S-H) gel phase and partly dissolved secondary phases [6]. The leaching
316 of iron was significantly higher than in any other mixture. It can be an indicator of the
317 stability of metallic oxides in aggressive conditions when incorporated in alkali-activated
318 matrices. This application has already been investigated by other authors [64-66], but further
319 work needs to be carried out to confirm the results in acid/aggressive environments. Although
320 the pictures obtained from SEM analyses (Figure 3) showed a common leaching front, the
321 EDT values are different (Table 4). As shown by the SEM mapping, the remaining aluminum,
322 silicon, and calcium contents in the damaged zone are still significant in the outer part of the
323 remaining section.

324 **Table 4.** Equivalent Damaged Thickness after 120 days for each element

EDT (µm)	**C3**	**AS**	**AM**	**AMF**
Sodium	7058	1419	1118	3021
Magnesium	496	293	0	0
Aluminium	412	251	145	307
Silicon	300	266	118	191
Calcium	707	737	110	627
Iron	260	200	12	13

325

326 A significant loss of aluminum took place in the AMF samples, which confirms the
327 weakening of the binder as the main damage mechanism. Compared to AM, the AMF mortar
328 appears to be more sensitive to the attack, with a possible contribution coming from partially
329 reacted fly ash particles that are subsequently dissolved in the acid solution. Previous studies
330 actually showed that significantly acid concentration promotes the extraction of aluminum
331 ions in the amorphous phase of high-alumina fly ash, and that Calcium and Sodium are
332 efficiently removed from fly ash [24]. Another particularity of the AMF samples is the high

amount of sodium that is released in the solution at the time of the first exposure (Fig. *5*). This behavior can be explained by significant content of free sodium cations that migrate easily to the surface of the samples before being transferred to the solution. This can be associated with the substitution of metakaolin with fly ash, a less reactive material with lower aluminum content, which results in an excess of sodium. The Al/Na ratio has been reported to have a significant influence on the mechanical properties of alkali-activated metakaolin, such as compressive strength and elastic modulus [67]. Moreover the specimens have been exposed to acid solution at relatively early age of 28 days, while the reactivity of fly ash is much slower than metakaolin. This results in significantly lower strength at 28 days, even if this material finally reaches equivalent strength at long-term [26]. The sodium cations are then more numerous than necessary for the electric equilibrium and thus more mobile.

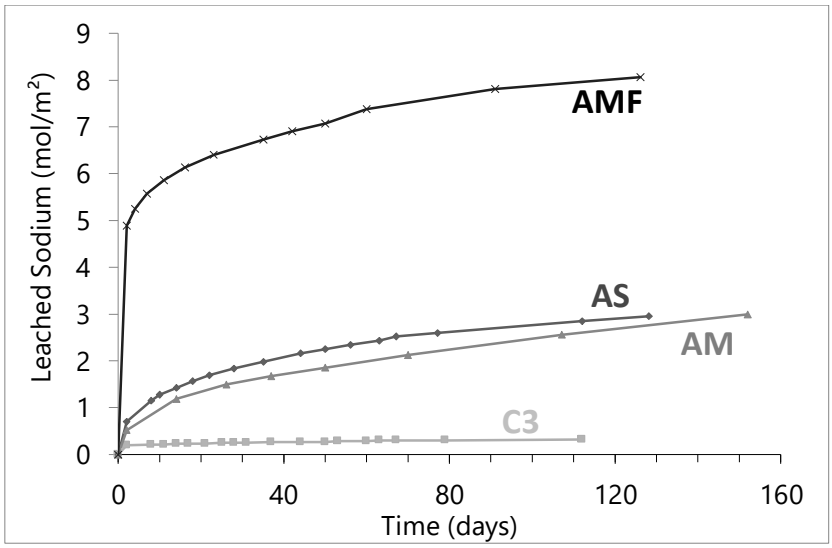

Fig. 5. Evolution of the leached sodium content

3.3 Correlations between chemical data and macroscopic behavior

The leaching behaviors of the samples characterized by the different elements globally agree with the previously described evolutions of the mass loss and volume variations. The main degradation mechanism seems to be the dissolution of the binding phases, i.e. calcium-

sodium-aluminosilicate (C-(A)-S-H) hydrates in the case of C3 and AS, and the aluminosilicate network present in AM and AMF. C-A-S-H and N-A-S-H gel are actually the main products of reactions in studied materials, depending on the calcium content and pH [19]. The nanostructure of studied alkali-activated metakaolin actually consists in polymerized 3D network where SiO_4 and AlO_4 tetrahedra are connected to 4 bridging oxygens linking it to silicon or aluminum atoms, as shown by solid-state nuclear magnetic resonance (NMR) spectra in another study [26]. Sodium silicate-activated slag can be described as a C-(A)-S-H gel with tobermorite of various levels of crosslinking [25]. Recent works have reported a decrease in the level of cross-linking at longer term, with higher structural organization of the C-A-S-H phase which suggests a later stage of aluminum incorporation in this phase [26]. Moreover C-A-S-H phase can coexist with polymerized N-A-S-(H) gel due to the structural limitations on Al substitution within the C-(N)-A-S-H gel and absence of Ca-rich phases [68].

This confirms that aluminum, silicon and calcium are the relevant elements for the assessment of the leaching kinetics and related nanostructural damage. Sodium leaching, however, does not appear to have a significant effect on the integrity of the materials. The corresponding EDTs were much higher than the other elements, signaling a higher diffusion rate through the matrix. Sodium ions are weakly bound in the nanostructure of N-A-S-H gel, where they balance the Al negative charges. Na can be leached out without affecting the strength of the material [27]. In the case of acid leaching, the negative charge can be compensated by the H_3O^+ ions provided by the solution.

In high-calcium binders, the leaching of hydroxide anions is driven by the dissolution of portlandite ($Ca(OH)_2$) [69]. The ratio between Ca^{2+} and OH^- concentrations in the leachate is generally around 2. Based on this observation, a quantity of positive charges has been calculated for the different mixtures, and correlated to the quantity of leached OH^-. The

cations considered are those belonging to the alkaline and alkaline earth metals groups, i.e. sodium, calcium and magnesium, each pondered by its respective charge. The quantity is then expressed in Equation 3.

$$\text{Cations} = n(Na^{+}) + 2n(Ca^{2+}) + 2n(Mg^{2+}) \qquad \text{Equation (3)}$$

Fig. *6* displays the evolution of Cations as a function of hydroxide anions. The first observation is a good correlation (R^2>0.99) for all the mixtures, showing that both components are ruled by the same mechanism and follow similar kinetics.

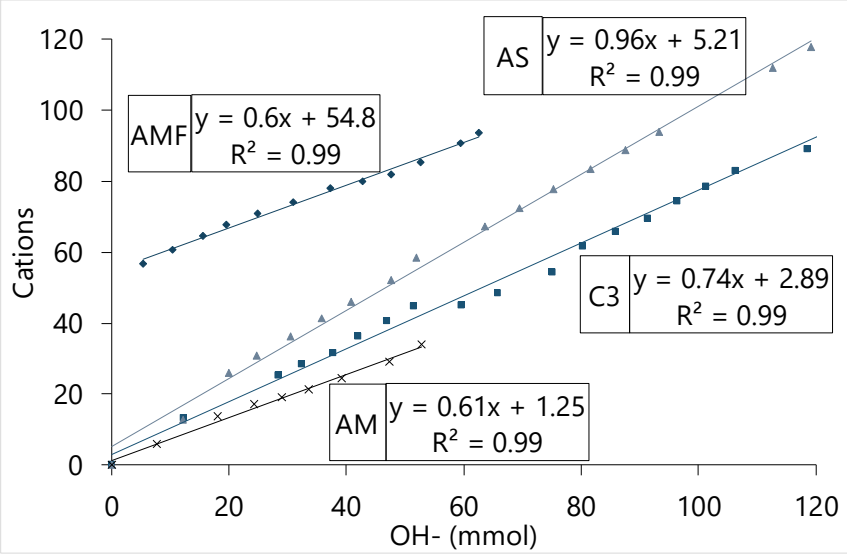

Fig. 6. Correlations between the leached cations and OH^-

For AS the Cations-to-hydroxide ratio is relatively high (~1), the value is lower for C3 and the other mixtures. For the geopolymer mortars, this can be attributed to the nature of the alkaline pore solution, where alkaline cations are associated to hydroxide anions [61]. Another explanation could be the dissociation of the hydroxyl groups present in the aluminosilicate network [69]. These ions are present either in terminal sites in the geopolymer chains or result from the ejection of aluminum tetrahedra after the acid attack. Allahverdi and Skvara suggested the steps of this process and its consequences in [23]. In the case of C-S-H structures found in hydrated cement [70], the exposition to acid environments causes the loss

of OH- ions and a deterioration of the chains due to their decalcification. The offset present in the AMF curve is related to the quantity of sodium released at the start of the experiment, as seen in Fig. *5*, then the ratio is exactly the same as AM.

Among the multiple correlations that can be investigated, the silicon-to-aluminum ratios are particularly interesting for the aluminosilicate materials. Fig. *7* shows a good correlation between the leached quantities of these two elements for the AM and AS samples.

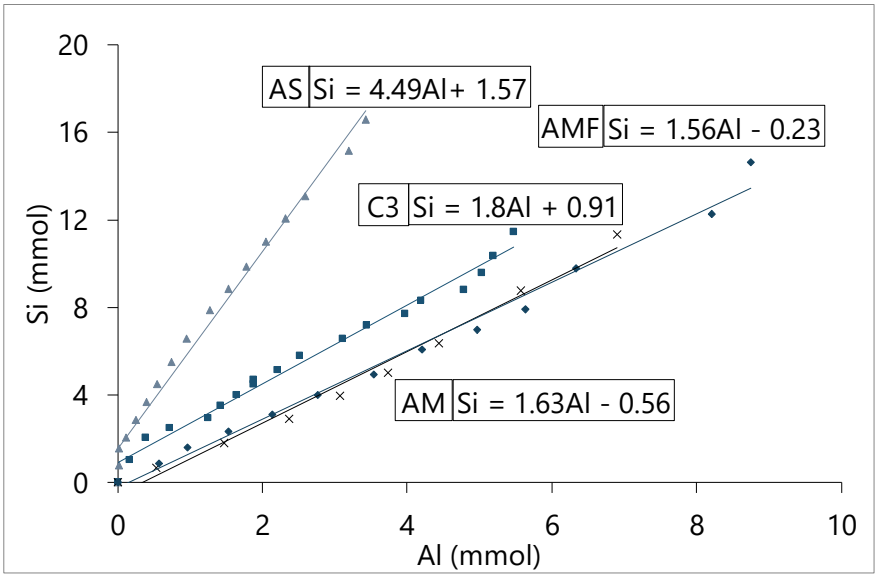

Fig. 7. Leached Si as a function of leached Al through time

Since they are generally associated in the matrix (the geopolymer network in AM [69] and the C-A-S-H gel in AS [25]), this pattern is expected. By comparing the slopes of the curves to the initial Si/Al ratios in both materials, some conclusions can be drawn. In AM, the initial theoretic ratio is 1.83, but the leaching produces Si and Al with a growing ratio that reaches 1.63 after 4 months. This is most likely because Al are released first due to the lower bond dissociation energy of the "Al-O-Si" bonds compared to the "Si-O-Si" bonds [71]. This results in a more siliceous network, as described in [23]. For the AS mixture, the leaching ratio is much closer to the initial Si/Al, which is 4.56. This shows that these two elements are mainly associated in the hydrate phases and are subjected to similar effects of the acid attack.

409 The degradation of the binder is then more uniform and it is mainly driven by the dissolution
410 of calcium which weakens the C-A-S-H structure [72]. In C3, the leached Si/Al ratio is much
411 lower than the initial ratio of the material (1.8 versus 2.86). This indicates that the aluminum
412 hydrates are more vulnerable to the attack and are thus more easily dissolved [73]. Combined
413 to the loss of calcium ensuing from the dissolution of portlandite, this fact leads to more
414 decalcified and poorly structured silicon products in the damaged zone [74].

415 Based on the initial compositions of the grouts, an equivalent volume composition can be
416 calculated for the mortars. It can be used to determine the volume of material loss by
417 converting the amounts of leached ions into dissolved volumes (Fig. *8*). This calculation
418 highlights the presence of an excess of leached calcium in C3 and AS for example, explained
419 by the presence of secondary hydrated phases.

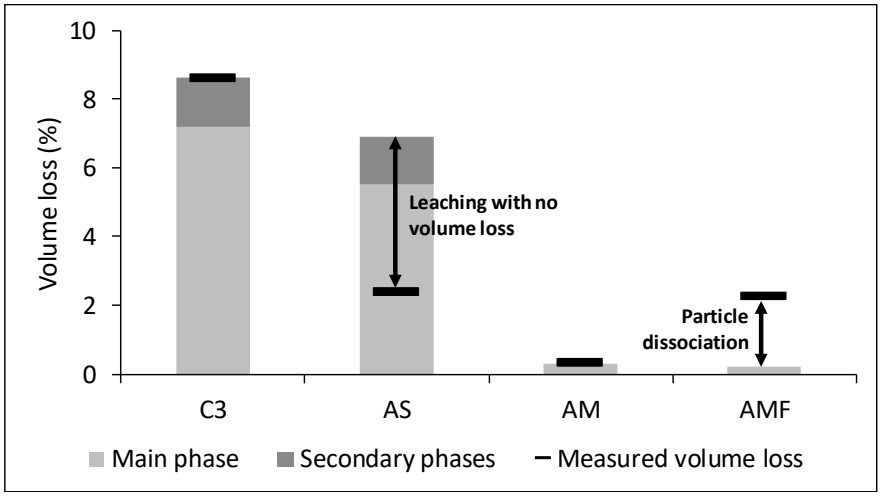

420

421 **Fig. 8.** Volume loss: calculated vs. measured

422 It also highlights the disproportionate amount of particles (sand and fly ash) that were
423 dissociated from the AMF sample and lead to a higher volume loss than predicted by
424 chemical calculations. The influence of curing methods on the strength development of alkali-
425 activated bottom ash has been investigated recently [75]. The authors concluded that seal
426 curing is more suitable, as the leaching of OH- and free alkali affects the strength

development. The strength of AMF samples could have been lower than expected due to leaching of activating solution while fly ash particles had not fully reacted. On the contrary, in the AS sample, the leached quantities of matter should have corresponded to a higher volume loss than the one measured. A possible modification in the density of the outer layer, with the formation of a lighter gel structure could explain this difference. Shi and Stegemann [30] have suggested the development of a protective gel layer that prevented the excessive corrosion of the material in the case of alkali-activated slag. This was confirmed by Sturm et al. [20]; silica gel precipitates at the mortar/acid interface, due to the low solubility of silica at low pH, inhibiting further degradation of the mortar. Bernal et al [34] mentioned an aluminosilicate type gel resulting from the decalcification of alkali-activated slag exposed to acetic acid at pH 4.5. In our study, there could be a similar phenomenon, with the formation of a barrier that slows the degradation of the binder, while still allowing the leaching of some elements. The measured volume via hydrostatic weighing would then show a lower value than predicted by the loss of matter.

4. Conclusion

The experimental study presented in this paper focuses on the resistance of cement-based and alkali-activated materials to acid leaching. A new combination of macroscopic and chemical indicators was proposed in order to understand the behavior of four binders, namely: slag cement, activated slag, activated metakaolin, and activated metakaolin with fly ash. The evolution of the global indicators and chemical analyses were associated with the direct observation of cross sections through SEM/EDS and X-ray microtomography. Based on the results presented in this paper the following conclusions can be drawn:

- At relatively low pH value of 3.5, the mortar mixture based on slag cement showed significant mass and volume losses, whereas activated metakaolin showed good

stability after 4-month exposure in controlled conditions. The performances of activated slag and activated metakaolin with fly ash were intermediate.

- Leaching resulted in a reduction of the cross section of exposed specimens. The remaining part of metakolin-based materials was physically sound, whereas slag-based materials showed a leaching front and a damaged depth attributable to the dissolution of calcium-rich phases.
- Whatever the binder composition, sodium was the most leachable element. However its release from binding phase did not result in significant damage of the material. This can be attributed to its replacement by H_3O^+ ions to balance the aluminates negative charges.
- The silicium-to-aluminium ratio of the leachate provides valuable information about the nature of hydration and alkali-activation products affected by leaching. Both elements are actually the main constituents of the binding phases, N-A-S-H or "geopolymer network" in activated metakaolin, and the C-A-S-H gel in activated slag.
- The amount of leached ions was converted into an equivalent mortar volume loss and compared with the direct measurement of the volume loss. This highlighted different behaviors of the studied materials which could not be predicted from their composition. It showed an excess of leached calcium for slag cement and activated slag, explained by the presence of secondary hydrated phases. Activated metakaolin with fly ash was characterized by a significant loss of sand and unreacted fly ash particles.

From the results of the study, materials based on activated metakaolin showed good performance at low pH values, for which cement-based materials cannot be directly exposed to acid solution. Although the replacement of metakaolin by fly ash could be valuable in terms of rheology or cost, it affected the resistance to leaching. Acid leaching should be

476 combined with other ions to investigate the behavior of alkali-activated materials in real
477 exposure conditions. This performance still needs to be associated to other engineering
478 properties and volume stability in order to recommend the use of these materials in severe
479 conditions.

480 **Acknowledgements**

481 The authors would like to thank Soletanche Bachy France and Ecole Centrale de Nantes for
482 their financial support and fruitful discussions.

483 **References**

484 [1] S. Kamali, B. Gerard, M. Moranville, Modelling the leaching kinetics of cement-based
485 materials—influence of materials and environment, Cement & Concrete Composites 25
486 (2003) 451–458

487 [2] D. Jacques, L. Wang, E. Martens, D. Mallants, Modelling chemical degradation of
488 concrete during leaching with rain and soil water types, Cem. Concr. Res. 40 (2010) 1306–
489 1313. doi:10.1016/j.cemconres.2010.02.008.

490 [3] F. Bernard, S. Kamali-Bernard, Performance simulation and quantitative analysis of
491 cement-based materials subjected to leaching, Computational Materials Science 50 (2010)
492 218–226

493 [4] T. Rougelot, N. Burlion, D. Bernard, F. Skoczylas, About microcracking due to leaching
494 in cementitious composites: X-ray microtomography description and numerical approach,
495 Cement and Concrete Research 40 (2010) 271–283

496 [5] B. Gérard, C. Le Bellego, O. Bernard, Simplified modelling of calcium leaching of
497 concrete in various environments, Mater. Struct. 35 (2002) 632–640.
498 doi:10.1007/BF02480356.

499 [6] T. De Larrard, F. Benboudjema, J.B. Colliat, J.M. Torrenti, F. Deleruyelle, Concrete
500 calcium leaching at variable temperature: Experimental data and numerical model inverse
501 identification, Comput. Mater. Sci. 49 (2010) 35–45. doi:10.1016/j.commatsci.2010.04.017.
502 [7] D.P. Bentz, E.J. Garboczi, Modeling the Leaching of Calcium Hydroxide From Cement
503 Paste - Effects on Pore-Space Percolation and Diffusivity, Mater. Struct. 25 (1992) 523–533.
504 doi:10.1007/bf02472448.
505 [8] D. Peak, J.W. Corbett, Diffusion-Controlled Reaction Kinetics, Phys. Rev. B. 5 (1972)
506 1226–1238. doi:10.1103/PhysRevB.5.1226.
507 [9] C. Carde, R. François, Effect of the leaching of calcium hydroxide from cement paste on
508 mechanical and physical properties, Cem. Concr. Res. 27 (1997) 539–550.
509 doi:10.1016/S0008-8846(97)00042-2.
510 [10] C. Carde, R. François, J.M. Torrenti, Leaching of both calcium hydroxide and C-S-H
511 from cement paste: Modeling the mechanical behavior, Cem. Concr. Res. 26 (1996) 1257–
512 1268. doi:10.1016/0008-8846(96)00095-6.
513 [11] R.E. Beddoe, H.W. Dorner, Modelling acid attack on concrete: Part I. The essential
514 mechanisms, Cem. Concr. Res. 35 (2005) 2333–2339. doi:10.1016/j.cemconres.2005.04.002.
515 [12] AFNOR, FD P 18-011 Béton Définition et classification des environnements
516 chimiquement agressifs - Recommandations pour la formulation des bétons, 11 (2016).
517 [13] N.I. Fattuni, B.P. Hughes, Effect of acid attack on concrete with different admixtures or
518 protective coatings, Cem. Concr. Res. 13 (1983) 655–665. doi:10.1016/0008-8846(83)90055-
519 8.
520 [14] J.G. Skousen, P.F. Ziemkiewicz, L.M. McDonald, Acid mine drainage formation, control
521 and treatment: Approaches and strategies, The Extractive Industries and Society 6 (2019)
522 241–249. doi.org/10.1016/j.exis.2018.09.008

523 [15] M.G. Sephton, J.A. Webb, Application of Portland cement to control acid mine drainage
524 generation from waste rocks, Applied Geochemistry 81 (2017) 143-154.
525 dx.doi.org/10.1016/j.apgeochem.2017.03.017

526 [16] J.L. Provis, Geopolymers and other alkali activated materials: why, how, and what?,
527 Mater. Struct. 47 (2014) 11–25. doi:10.1617/s11527-013-0211-5.

528 [17] C. Grengg, F. Mittermayr, N. Ukrainczyk, G. Koraimann, S. Kienesberger, M. Dietzel,
529 Advances in concrete materials for sewer systems affected by microbial induced concrete
530 corrosion: A review, Water Research 134 (2018) 341-352

531 [18] W. Zhang, X. Yao, T. Yang, Z. Zhang, The degradation mechanisms of alkali-activated
532 fly ash/slag blend cements exposed to sulphuric acid, Construction and Building Materials
533 186 (2018) 1177–1187. doi.org/10.1016/j.conbuildmat.2018.08.050

534 [19] I. Garcia-Lodeiro, A. Palomo, A. Fernández-Jiménez, D.E. Macphee, Compatibility
535 studies between N-A-S-H and C-A-S-H gels. Study in the ternary diagram Na2O–CaO–
536 Al2O3–SiO2–H2O, Cem. Concr. Res. 41 (2011) 923–931.
537 doi:10.1016/j.cemconres.2011.05.006.

538 [20] P. Sturm, G.J.G. Gluth, C. Jäger, H.J.H. Brouwers, H.-C. Kühne, Sulfuric acid resistance
539 of one-part alkali-activated mortars, Cement and Concrete Research 109 (2018) 54–63.
540 https://doi.org/10.1016/j.cemconres.2018.04.009

541 [21] M. Mainguy, C. Tognazzi, J.-M. Torrenti, F. Adenot, Modelling of leaching in pure
542 cement paste and mortar, Cement and Concrete Research 30 (2000) 83–90.

543 [22] E.Rozière, A.Loukili, R. El-Hachem, F. Grondin, Durability of concrete exposed to
544 leaching and external sulphate attack, Cement and Concrete Research, 39 (12), p. 1188-1198,
545 2009

546 [13] A. Allahverdi, F. Škvára, Nitric acid attack on hardened paste of geopolymeric cements,
547 Ceram. - Silikaty. 45 (2001) 143–149. doi:10.1016/S0167-577X(02)01009-1.

548 [24] J.B. Zhang, S.-P. Li, H.-Q. Li, M.-M. He, Acid activation for pre-desilicated high-
549 alumina fly ash, Fuel Processing Technology 151 (2016) 64–71

550 [25] R.J. Myers, S.A. Bernal, R. San Nicolas, J.L. Provis, Generalized structural description
551 of calcium-sodium aluminosilicate hydrate gels: the cross-linked substituted tobermorite
552 model., Langmuir. 29 (2013) 5294–306. doi:10.1021/la4000473.

553 [26] A. Cherki El Idrissi, M. Paris, E. Rozière, D. Deneele, S. Darson, A. Loukili, Alkali-
554 activated grouts with incorporated fly ash: From NMR analysis to mechanical properties,
555 Materials Today Communications 14 (2018) 225–232, doi:10.1016/j.mtcomm.2018.01.012

556 [27] F. Škvára, V. Šmilauer, P. Hlaváček, L. Kopecký, Z. Cílová, A Weak Alkali Bond In (N,
557 K)–A–S–H Gels: Evidence From Leaching and Modeling,, Ceramics – Silikáty 56 (4) 374-
558 382 (2012)

559 [28] A. Koenig, A. Herrmann, S. Overmann, F. Dehn, Resistance of alkali-activated binders
560 to organic acid attack: Assessment of evaluation criteria and damage mechanisms,
561 Construction and Building Materials 151 (2017) 405–413.
562 doi.org/10.1016/j.conbuildmat.2017.06.117

563 [29] R.R. Lloyd, J.L. Provis, J.S.J. Deventer, Acid resistance of inorganic polymer binders. 1.
564 Corrosion rate, Mater. Struct. 45 (2012) 1–14. doi:10.1617/s11527-011-9744-7.

565 [30] A. Mellado, M.I. Pérez-Ramos, J. Monzó, M.V. Borrachero, J. Payá, Resistance to acid
566 attack of alkali-activated binders: Simple new techniques to measure susceptibility,
567 Construction and Building Materials 150 (2017) 355–366

568 [31] T. Bakharev, Resistance of geopolymer materials to acid attack, Cem. Concr. Res. 35
569 (2005) 658–670. doi:10.1016/j.cemconres.2004.06.005.

570 [32] A. Allahverdi, F. Škvára, Sulfuric acid attack on hardened paste of geopolymer cements
571 part 1. Mechanism of corrosion at relatively high concentrations, Ceram. - Silikaty. 49 (2005)
572 225–229. doi:10.1016/S0167-577X(02)01009-1.

573 [33] T. Bakharev, J.G. Sanjayan, Y.-B. Cheng, Resistance of alkali-activated slag concrete to
574 acid attack, Cement and Concrete Research 33 (2003) 1607– 1611

575 [34] S.A. Bernal, E.D. Rodríguez, R. Mejía de Gutiérrez & J.L. Provis (2012) Performance of
576 alkali-activated slag mortars exposed to acids, Journal of Sustainable Cement-Based
577 Materials, 1:3, 138-151, DOI: 10.1080/21650373.2012.747235

578 [35] A. Koenig, F. Dehn, Main considerations for the determination and evaluation of the acid
579 resistance of cementitious materials, Materials and Structures (2016) 49:1693–1703. DOI
580 10.1617/s11527-015-0605-7

581 [36] E. Gruyaert, P. Van den Heede, M. Maes, N. De Belie, Investigation of the influence of
582 blast-furnace slag on the resistance of concrete against organic acid or sulphate attack by
583 means of accelerated degradation tests, Cement and Concrete Research 42 (2012) 173–185.
584 doi:10.1016/j.cemconres.2011.09.009

585 [37] Y. Xie, X. Lin, W. Pan, T. Ji, Y. Liang, H. Zhang, Study on corrosion mechanism of
586 alkali-activated concrete with biogenic sulfuric acid, Construction and Building Materials 188
587 (2018) 9–16. doi.org/10.1016/j.conbuildmat.2018.08.105

588 [38] L. Gu, T. Bennett, P. Visintin, Sulphuric acid exposure of conventional concrete and
589 alkali-activated concrete: Assessment of test methodologies, Construction and Building
590 Materials 197 (2019) 681–692. doi.org/10.1016/j.conbuildmat.2018.11.166

591 [39] M. Vafaei, A. Allahverdi, P. Dong, N. Bassim, Acid attack on geopolymer cement
592 mortar based on waste-glass powder and calcium aluminate cement at mild concentration,
593 Construction and Building Materials 193 (2018) 363–372.
594 doi.org/10.1016/j.conbuildmat.2018.10.203

595 [40] J. Zhang, C. Shi, Z. Zhang, Z. Ou, Durability of alkali-activated materials in aggressive
596 environments: A review on recent studies, Construction and Building Materials 152 (2017)
597 598–613. doi.org/10.1016/j.conbuildmat.2017.07.027

598 [41] A. Allahverdi, F. Škvára, Sulfuric acid attack on hardened paste of geopolymer cements
599 Part 2. Corrosion mechanism at mild and relatively low concentrations, Ceram. - Silikaty. 50
600 (2006) 1–4. doi:10.1016/S0167-577X(02)01009-1.
601 [42] A. Keulen, A. van Zomeren, J.J. Dijkstra, Leaching of monolithic and granular alkali
602 activated slag-fly ash materials, as a function of the mixture design, Waste Management 78
603 (2018) 497–508. doi.org/10.1016/j.wasman.2018.06.019
604 [43] D. Wang, Q. Wang, S. Zhuang, J. Yang, Evaluation of alkali-activated blast furnace
605 ferronickel slag as a cementitious material: Reaction mechanism, engineering properties and
606 leaching behaviors, Construction and Building Materials 188 (2018) 860–873
607 [44] K. Gijbels, S. Landsberger, P. Samyn, R. Ion Iacobescud, Y. Pontikes, S. Schreurs,W.
608 Schroeyers, Radiological and non-radiological leaching assessment of alkali-activated
609 materials containing ground granulated blast furnace slag and phosphogypsum, Science of the
610 Total Environment 660 (2019) 1098–1107
611 [45] M. Reza Azadi, A. Taghichian, A. Taheri, Optimization of cement-based grouts using
612 chemical additives, Journal of Rock Mechanics and Geotechnical Engineering 9 (2017) 623-
613 637. dx.doi.org/10.1016/j.jrmge.2016.11.013
614 [46] T.H. Phan, M. Chaouche, M. Moranville, Influence of organic admixtures on the
615 rheological behavior of cement pastes, Cement and Concrete Research 36 (2006) 1807–1813.
616 doi:10.1016/j.cemconres.2006.05.028
617 [47] S. Li, F. Sha, R. Liu, Q. Zhang, Z. Li, Investigation on fundamental properties of
618 microfine cement and cement-slag grouts, Construction and Building Materials 153 (2017)
619 965–974. dx.doi.org/10.1016/j.conbuildmat.2017.05.188
620 [48] K. Haga, S. Sutoua, M. Hironaga, S. Tanaka, Shinya Nagasaki, Effects of porosity on
621 leaching of Ca from hardened ordinary Portland cement paste, Cement and Concrete Research
622 35 (2005) 1764– 1775. doi:10.1016/j.cemconres.2004.06.034

623 [49] N. Cristelo, E. Soares, I. Rosa, T. Miranda, D.V. Oliveira, R. Silva & A. Chaves,
624 Rheological properties of alkaline activated fly ash used in jet grouting applications.
625 Construction and Building Materials, 48 (2013) 925–933.
626 doi.org/10.1016/j.conbuildmat.2013.07.063
627 [50] M. Romagnoli, C. Leonelli, E. Kamse, & M. Lassinantti Gualtieri, Rheology of
628 geopolymer by DOE approach. Construction and Building Materials, 36 (2012) 251–258.
629 dx.doi.org/10.1016/j.conbuildmat.2012.04.122
630 [51] A.I. Laskar and R. Bhattacharjee, Effect of Plasticizer and Superplasticizer on Rheology
631 of Fly-Ash-Based Geopolymer Concrete, ACI Materials Journal, 110-M46 (2013) 513-518
632 [52] E. Rozière, A. Loukili, Performance-based assessment of concrete resistance to leaching,
633 Cem. Concr. Compos. 33 (2011) 451–456. doi:10.1016/j.cemconcomp.2011.02.002.
634 [53] A. Aboulayt, R. Jaafri, H. Samouh, A. Cherki El Idrissi, E. Roziere, R. Moussa, A.
635 Loukili, Stability of a new geopolymer grout: Rheological and mechanical performances of
636 metakaolin-fly ash binary mixtures, Construction and Building Materials 181 (2018) 420–436
637 [54] C. Badoz, P. Francisco, P. Rougeau, A Performance Test to Estimate Durability of
638 Concrete Products Exposed to Chemical Attacks, Fédération Internationale du Béton,
639 Proceedings of the 2nd International Congress, June 5-8, 2006 – Naples, Italy
640 [55] R. El-Hachem, E. Rozière, F. Grondin, A. Loukili, Multi-criteria analysis of the
641 mechanism of degradation of Portland cement based mortars exposed to external sulphate
642 attack, Cement and Concrete Research, 42 (10), p 1327-1335, 2012
643 [56] X.X. Gao, P. Michaud, E. Joussein, S. Rossignol, Behavior of metakaolin-based
644 potassium geopolymers in acidic solutions, J. Non. Cryst. Solids. 380 (2013) 95–102.
645 doi:10.1016/j.jnoncrysol.2013.09.002.

646 [57] Z. Zhang, H. Wang, Y. Zhu, A. Reid, J.L. Provis, F. Bullen, Using fly ash to partially
647 substitute metakaolin in geopolymer synthesis, Appl. Clay Sci. 88–89 (2014) 194–201.
648 doi:10.1016/j.clay.2013.12.025.

649 [58] C. Shi, A. Fernandez-Jimenez, Stabilization/solidification of hazardous and radioactive
650 wastes with alkali-activated cements, Journal of Hazardous Materials, 137 (2006) 1656–1663

651 [59] C. Shi, J.. Stegemann, Acid corrosion resistance of different cementing materials, Cem.
652 Concr. Res. 30 (2000) 803–808. doi:10.1016/S0008-8846(00)00234-9.

653 [60] M. Moranville, S. Kamali, E. Guillon, Physicochemical equilibria of cement-based
654 materials in aggressive environments—experiment and modeling, Cem. Concr. Res. 34
655 (2004) 1569–1578. doi:10.1016/j.cemconres.2004.04.033

656 [61] R.R. Lloyd, J.L. Provis, J.S.J. van Deventer, Pore solution composition and alkali
657 diffusion in inorganic polymer cement, Cem. Concr. Res. 40 (2010) 1386–1392.
658 doi:10.1016/j.cemconres.2010.04.008.

659 [62] P. Duxson, G.C. Lukey, F. Separovic, J.S.J. Van Deventer, Effect of alkali cations on
660 aluminum incorporation in geopolymeric gels, Ind. Eng. Chem. Res. 44 (2005) 832–839.
661 doi:10.1021/ie0494216.

662 [63] Z. Aly, E.R.R. Vance, D.S.S. Perera, Aqueous dissolution of sodium aluminosilicate
663 geopolymers derived from metakaolin, J. Nucl. Mater. 424 (2012) 164–170.
664 doi:10.1016/j.jnucmat.2012.02.027.

665 [64] J.G.S. Van Jaarsveld, J.S.J. Van Deventer, A. Schwartzman, The potential use of
666 geopolymeric materials to immobilise toxic metals: Part II. Material and leaching

667 [65] J.G.S. Van Jaarsveld, J.S.J. Van Deventer, G.C. Lukey, A Comparative Study of
668 Kaolinite Versus Metakaolinite in Fly Ash Based Geopolymers Containing Immobilized
669 Metals, Chem. Eng. Commun. 191 (2004) 531–549. doi:10.1080/00986440490277974.

670 [66] M. Cyr, R. Idir, G. Escadeillas, Use of metakaolin to stabilize sewage sludge ash and
671 municipal solid waste incineration fly ash in cement-based materials, J. Hazard. Mater. 243
672 (2012) 193–203. doi:10.1016/j.jhazmat.2012.10.019.

673 [67] A. Cherki El Idrissi, E. Roziere, A. Loukili and S. Darson, European Journal of
674 Environmental and Civil Engineering, 2018, Vol. 22, No. 5, 628–649,
675 doi:10.1080/19648189.2016.1214183

676 [68] B. Walkley, R. San Nicolas, M.-A. Sani, G.J. Rees, J.V. Hanna, J.S.J. van Deventer, J.L.
677 Provis Phase evolution of C-(N)-A-S-H/N-A-S-H gel blends investigated via alkali activation
678 of synthetic calcium aluminosilicate precursors. Cem Concr Res 89 (2016) 120–135

679 [69] V.F.F. Barbosa, K.J.D. MacKenzie, C. Thaumaturgo, Synthesis and characterisation of
680 materials based on inorganic polymers of alumina and silica: Sodium polysialate polymers,
681 Int. J. Inorg. Mater. 2 (2000) 309–317.

682 [70] I.G. Richardson, The calcium silicate hydrates, Cem. Concr. Res. 38 (2008) 137–158.
683 doi:10.1016/j.cemconres.2007.11.005.

684 [71] Y.-R. Luo, Bond dissociation energies, in: CRC Handb. Chem. Phys., 2007: pp. 65–98.

685 [72] T. Bakharev, J. Sanjayan, Y.-B. Cheng, Resistance of alkali-activated slag concrete to
686 acid attack, Cem. Concr. Res. 33 (2003) 1607–1611. doi:10.1016/S0008-8846(03)00125-X.

687 [73] A. Allahverdi, F. Skvara, Acidic corrosion of hydrated cement based materials - Part 1,
688 Ceram. – Silikáty. 3 (2000) 114–120.

689 [74] V. Pavlík, Corrosion of hardened cement paste by acetic and nitric acids part II:
690 Formation and chemical composition of the corrosion products layer, Cem. Concr. Res. 24
691 (1994) 1495–1508. doi:10.1016/0008-8846(94)90164-3.

692 [75] G. Huang, Y. Ji, L. Zhang, J. Li, Z. Hou, The influence of curing methods on the strength
693 of MSWI bottom ash-based alkali-activated mortars: The role of leaching of OH and free
694 alkali, Construction and Building Materials 186 (2018) 978–985